SCIENCE CHINA
Technological Sciences

Special Topic: 4D Printing of Stimuli-Responsive Materials
•Article•

April 2020 Vol.63 No.4: 578–588
https://doi.org/10.1007/s11431-019-1468-2

4D printing of personalized shape memory polymer vascular stents with negative Poisson's ratio structure: A preliminary study

LIN Cheng[1†], ZHANG LiJin[1†], LIU YanJu[1], LIU LiWu[1*] & LENG JinSong[2*]

[1] *Department of Astronautic Science and Mechanics, Harbin Institute of Technology (HIT), Harbin 150001, China;*
[2] *National Key Laboratory of Science and Technology on Advanced Composites in Special Environments, Harbin Institute of Technology (HIT), Harbin 150080, China*

Received July 17, 2019; accepted October 17, 2019; published online February 28, 2020

Four-dimensional (4D) printing, integrates transformation information into three-dimensional (3D)-printed structures, which means that 3D-printed structures are able to change their shapes, properties, or functionalities over time. Here, two types of shape memory personalized vascular stents with negative Poisson's ratio structure are developed via 4D printing. The genetic algorithm is used to optimize the structure. Axial compression tests, radial compression tests and three-point bending tests are carried out to study the mechanical properties of the stents. In addition, fluid-structure interaction and stress distribution during the shape recovery process are investigated based on finite element method. The shape memory behaviors of the stents are excellent and *in vitro* feasibility tests demonstrate that the stents can expand the simulated narrow blood vessel rapidly. Therefore, 4D printed shape memory stents with negative Poisson's ratio structure are highly promising for the treatment of vascular stenosis.

shape memory polymer, 4D printing, biodegradable vascular stents, finite element analysis, negative Poisson's ratio

Citation: Lin C, Zhang L J, Liu Y J, et al. 4D printing of personalized shape memory polymer vascular stents with negative Poisson's ratio structure: A preliminary study. Sci China Tech Sci, 2020, 63: 578–588, https://doi.org/10.1007/s11431-019-1468-2

1 Introduction

Shape memory polymers (SMPs), a type of stimuli-responsive material, are able to recover to their original shape from a deformed shape under external stimuli [1–4]. Due to the adjustable properties and changeable structures, SMPs have captured extensive attention in biomedical field [5–13]. Zhao et al. [14] designed shape memory scaffolds via electrospinning technology, the cells can easily attach to the 2D surface of the scaffolds and then rolled into a 3D structure automatically, providing a facile 3D endothelialization method. However, the structure of medical devices is usually complicated, and some even need to be customized for specific patients. The complex structure is far beyond the capability of traditional manufacturing technology, which makes the manufacturing process costly and time-consuming. Three-dimensional (3D) printing, also known as additive manufacturing has provided new opportunities for preparing these medical architectures. 3D printing has shown immense potential applications in medical field, such as bone tissue engineering [15–18], neural tissue models [19], drug products [20,21] and scaffolds [22,23]. With the combination of 3D printing and smart materials (e.g., shape memory polymers), the 3D printed structures can change their shapes and properties with time when exposed to stimuli [24,25]. Therefore, this leads to a new concept of four-dimensional (4D) printing, which integrates time with 3D printing as the fourth dimension. This is a more intelligent way of manufacturing medical devices with self-assembly and multifunctional characteristics [26,27]. Zarek et al. [28] fabricated customized shape memory endoluminal scaffolds via 4D

†These authors contributed equally to this work.
*Corresponding authors (email: liuliwu_006@163.com; lengjs@hit.edu.cn)

printing. The customized structure largely avoided the possibility of migration and ensured stable fixation.

Recently, the incidence of vascular stenosis has continuously increased, which seriously threatens people's health [29]. Stenosis refers to the lumen narrows of the arteries, resulting from atherosclerosis, in which plaques form on the inner wall of the arteries. Figure 1 is a schematic of a narrow artery and the narrow artery after stent deployment. Since Sigwart et al. [30] first implanted a metal stent in human body by an interventional therapy in 1986, stent placement has been increasingly accepted as an effective treatment for stenosis due to the reduced scarring, high efficiency and rapid recovery [31,32]. Later, metal stents, such as stainless steel stents, tantalum stents, and nickel-titanium-chromium alloy stents, have been widely used clinically [33]. However, non-degradable metal stents remain in the blood vessels permanently, which increases the risk of chronic damage to vessels and intimal smooth muscle cell proliferation, leading to restenosis. In this case, biodegradable stents have emerged as a good alternative to metal stents, which can reduce thrombosis, prevent restenosis and avoid other complications [6].

Negative Poisson's ratio (NPR, also known as auxetic) structures have attracted significant attention due to their excellent properties, such as lightweight and high specific stiffness [34,35]. Therefore, when NPR structure is applied to vascular stents, stents can provide higher strength at lower surface coverage. In addition, NPR structures can expand (contract) in transverse directions when subjected to uniaxial tension (compression). This means that stents with NPR structure possess a high contraction-expansion ratio, facilitating minimally invasive deployment. There are some studies on vascular stents [36,37]; however, the investigation of SMP-based vascular stents with NPR structures are far from fully explored.

Here, personalized shape memory vascular stents with different numbers of NPR structural units were developed using 4D printing. Shape memory polylactic acid (PLA) was selected as the printing material due to the excellent properties such as high modulus and tensile strength, biodegradability, biocompatibility, outstanding processability and shape memory effect. The structure was optimized by genetic algorithm and the mechanical performances of the stents were investigated based on both finite element methods and experiments. In addition, shape recovery properties and *in vitro* feasibility study were examined.

2 Models and simulations

2.1 Structure design and optimization

Shape memory polymer vascular stents with NPR structure were developed considering 25% vascular stenosis (Figure 1). Figure 2 depicts the unit cells of the vascular stent before and after optimization, as well as the definition of geometric parameters. The initial values were: l=0.7 mm, h=1.3 mm, t =0.1 mm and θ=20°.

The mechanical properties of NPR honeycomb structures are strongly associated with their geometry. Since the pioneering work of Adeli and Cheng [38] in 1993, the genetic algorithm has been widely used in structure design optimization [39]. According to the Gibson theory [40], the Young's modulus in the horizontal direction (E_1), Young's modulus in the vertical direction (E_2) and in-plane shear modulus (G_{12}) of the concave hexagonal NPR structure are as follows:

$$E_1 = E_0\left(\frac{t}{l}\right)^3 \frac{\cos\theta}{(h/l+\sin\theta)\sin^2\theta}, \tag{1}$$

$$E_2 = E_0\left(\frac{t}{l}\right)^3 \frac{(h/l+\sin\theta)}{\cos^3\theta}, \tag{2}$$

$$G_{12} = E_0\left(\frac{t}{l}\right)^3 \frac{(h/l+\sin\theta)}{(h/l)^2(1+2h/l)\cos\theta}, \tag{3}$$

where l, h, t and θ are size parameters in Figure 2. E_0 is the elastic modulus of the raw material, which is calculated according to the stress-strain curve of shape memory PLA in Figure 3(a). To characterize the mechanical properties comprehensively, the weighted summation method was used to obtain the comprehensive performance expression (objective function) f [41], which was calculated according to

$$f = 0.048E_1 + 0.476E_2 + 0.476G_{12}. \tag{4}$$

The objective function f was optimized using genetic algorithm, and Figure 3(b) shows the genetic algorithm optimization flowchart [39]. The relationship between the

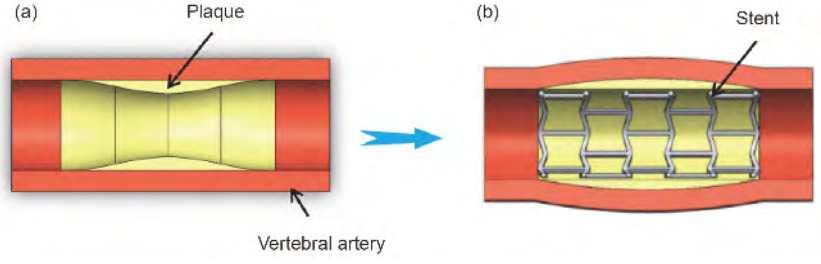

Figure 1 (Color online) Schematic illustrations of a narrow artery (a) and a narrow artery after stent deployment (b).

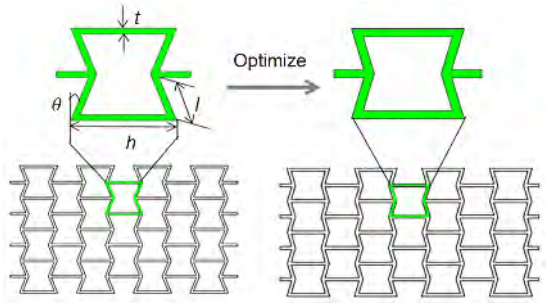

Figure 2 (Color online) Unit cells before and after optimization.

chromosome and the objective function was coded first, and the size parameters of the honeycomb unit cell were regarded as the chromosomes. Then, chromosomes were encoded to binary genes to generate the initial population. The number of individuals was set to 200 and the maximum number of iterations was set to 150. The fitness of the population was calculated. The crossover and mutation operations were performed in the solution space with a crossover probability of 0.9 and a mutation probability of 0.01. The range values of variables are t=0.08–0.12 mm, l=0.78–1.37 mm, h=0.65–1.14 mm and θ=15°–30°. The offspring was reproduced until optimal solution output. After about 50 generations of inheritance, the solution tended to be stable.

After optimization by genetic algorithm, the optimal structural parameters that can make the objective function obtain the maximum value were: l=0.65 mm, h=1.37 mm, t=0.12 mm and θ=15°. To verify the mechanical properties before and after structural optimization, finite element simulations were carried out under three loading conditions, including axial tensile load in X and Y directions and shear load. The distributions of stress and displacement were obtained and analyzed to calculate the elastic modulus (E_1, E_2) and shear modulus (G_{12}). The distributions of stress and displacement under the three types of loading are shown in Figures S1–S3 (Supporting Information). The maximum stress and strain values before and after structure optimization are listed in Table S1. Figure 2(c) is the comparison of mechanical parameters before and after optimization, the three parameters were significantly improved. E_1 and E_2 increased by more than 3 times, and G_{12} increased by 2 times.

With the optimized unit cell, two types of topology structures were designed. Figure 4(a) and (b) is the unfolded plane geometries of the Type 1 stent and the Type 2 stent with 21.4% and 21.1% surface coverage, respectively. Three-dimensional models of the stents were obtained by bending the unfolded plane geometries (Figure 4(b) and (e)).

2.2 Fluid-structure interaction analysis

To consider the influence of blood flow on the stent and blood vessel in the physical microenvironment after implantation, the fluid-solid coupling analysis was performed using the MECHANICAL and FLUENT solvers in ANSYS. Models of plaques and blood vessel with an occlusion rate of

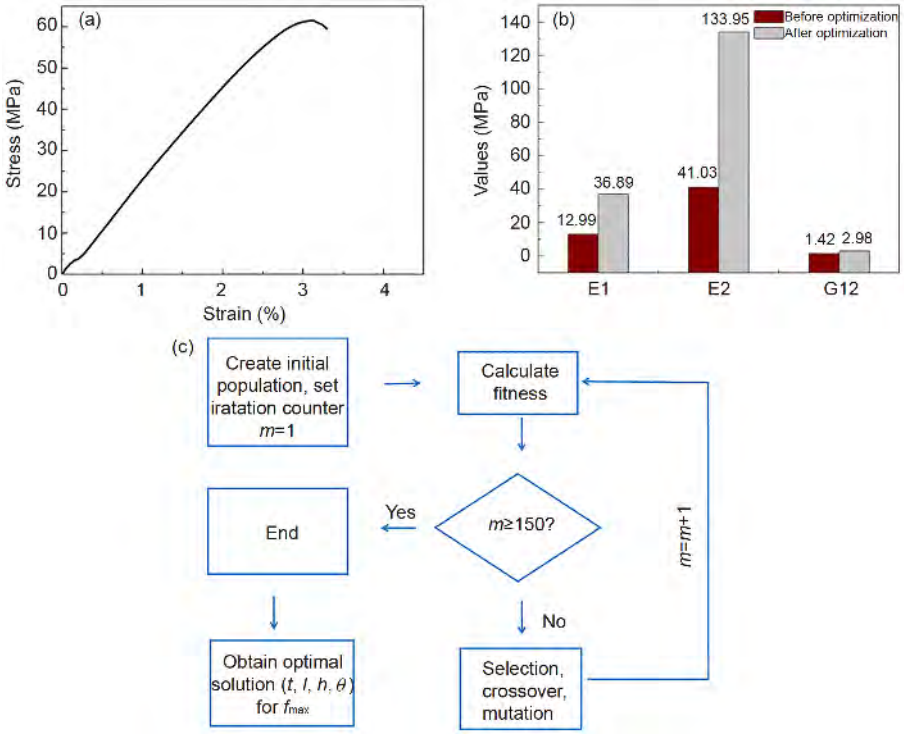

Figure 3 (Color online) (a) Standard specimens tensile tests of shape memory PLA; (b) genetic algorithm optimization flowchart; (c) comparison of mechanical parameters before and after optimization.

25% were established. The blood flow rate was 60 cm/s and the blood pressure was 140 mmHg (1 mmHg=133.322 Pa). The detailed parameters are displayed in Table S2. The turbulence effect was considered, and the turbulent flow energy and the dissipation rate were set as 0.02 m^2/s^2 and 0.5 m^2/s^3. The flow field results and the kinetic energy diagram of the fluid-solid coupling action surface are shown in Figure S4.

Equivalent stress distribution and deformation distribution of the stents are shown in Figure 5. The values of maximum stress and displacement are displayed in Table S3. The maximum equivalent stress and maximum shear stress of the Type 1 stents were 0.68 and 0.093 MPa, respectively. Those of the Type 2 stents were slightly smaller, 0.35 and 0.047 MPa, respectively. The maximum deformation of the Type 1 stent (3.56×10^{-6} m) was less than that of the Type 2 stent (4.495×10^{-6} m).

2.3 Shape memory behavior characterization based on finite element analysis

Shape memory polymer is a kind of viscoelastic material that exhibits both viscosity and elasticity, and its modulus changes with temperature and time. Therefore, factors such as loading conditions, temperature, and time, will affect the

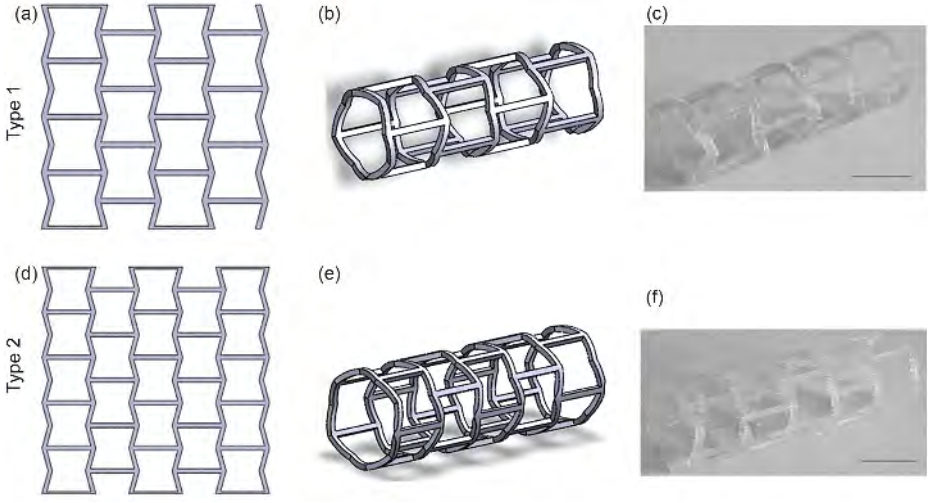

Figure 4 (Color online) Schematic of the two types of stents. (a) Unfolded plane geometry of Type 1 stent; (b) three-dimensional model of Type 1 stent; (c) 4D printed Type 1 stent; (d) unfolded plane geometry of Type 2 stent; (e) three-dimensional model of Type 2 stent; (f) 4D printed Type 2 stent.

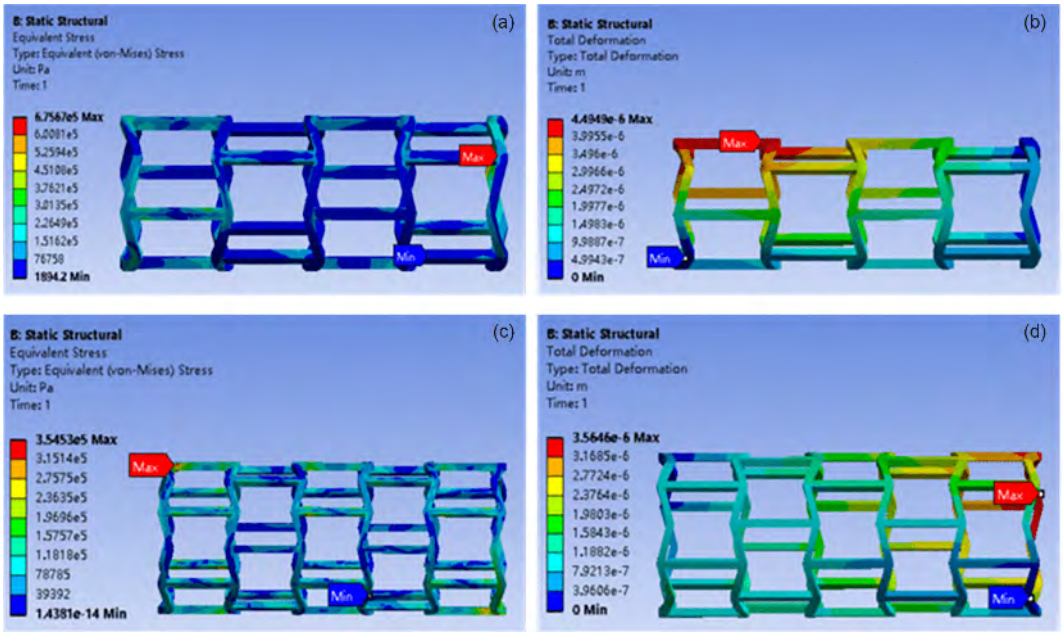

Figure 5 (Color online) Distributions of equivalent stress and deformation based on fluid-structure interaction. (a) Equivalent stress distribution of Type 1 stent; (b) deformation distribution of Type 1 stent; (c) equivalent stress distribution of Type 2 stent; (d) deformation distribution of Type 2 stent.

deformation process. The generalized Maxwell model is generally used to describe the viscoelastic property of shape memory polymer, the constitutive models are as follows [42]:

$$\sigma(t)=\int_0^t 2G(\tau-\tau')\dot{\mathbf{e}}\mathrm{d}t'+\mathbf{I}\int_0^t K(\tau-\tau')\dot{\phi}\mathrm{d}t', \tag{5}$$

where σ is the instantaneous Cauchy stress, $G(t)$ and $K(t)$ represent the small-strain shear and bulk relaxation moduli, and τ is the reduced time.

Eq. (5) can be transformed into the following form:

$$\sigma(t)=2G_0\mathbf{e}(t)+\int_0^\tau 2\dot{G}(\tau')\mathbf{e}(t-t')\mathrm{d}\tau' +\mathbf{I}(K_0\varnothing(t)+\int_0^\tau \dot{K}(\tau')\varnothing(t-t')\mathrm{d}\tau'), \tag{6}$$

where G_0 and K_0 are the instantaneous shear and bulk moduli, $\mathbf{e}$ and $\varnothing$ represent the mechanical deviatoric and volumetric strains.

The expressions of the Prony series used to describe small-strain relaxation moduli $G(t)$ and $K(t)$ in ABAQUS software are as follows:

$$G(t)=G_0\left[\alpha_\infty^{\ G}+\sum_{i=1}^{n_G}\alpha_i^{\ G}\exp\left(-t/\tau_i^{\ G}\right)\right], \tag{7a}$$

$$G_0=G(t=0)=G_\infty+\sum_{i=1}^{n_G}G_i, \tag{7b}$$

$$K(t)=K_0\left[\alpha_\infty^{\ K}+\sum_{i=1}^{n_K}\alpha_i^{\ K}\exp\left(-t/\tau_i^{\ K}\right)\right], \tag{8a}$$

$$K_0=K(t=0)=K_\infty+\sum_{i=1}^{n_K}K_i, \tag{8b}$$

where K_∞ and G_∞ are shear and bulk moduli at time $t=\infty$.

Time-temperature superposition shifting factor (a_T) is determined by Williams-Landel-Ferry (WLF) equation [43]:

$$\log a_T=-\frac{C_1(T-T_M)}{C_2+(T-T_M)}, \tag{9}$$

where T_M is the reference temperature. C_1 and C_2 are material constants, which depends on T_M. The parameters in the shape memory simulation process are listed in Table S4.

The shape memory process of shape memory PLA can be described as the following four stages. (1) Programming stage. When the temperature is below the glass transition temperature (T_g), PLA is in the glassy state. When it is heated above T_g, it enters a rubbery state and becomes soft. Hence, its structure can be deformed into any temporary shape under external load. (2) Cooling stage. The structure is cooled below T_g and the temperature is maintained for a period of time to fix the temporary shape. (3) Unloading stage. The external load is removed. (4) Recovering stage. When re-heated above T_g, the structure automatically recovers to its original shape. More details about shape memory mechanisms can be found in ref. [44].

The shape memory process of the stents was simulated by ABAQUS software. During the programming stage, axial and radial displacement loads were simultaneously applied to the stents to obtain the temporary shape of the stents (Figure 6(a) and (b)). The maximum stress and maximum strain distributions over time are shown in Figure 6, which is difficult to access experimentally. The recovery process was uniform and the stresses at the connection points were relatively high. Figure 7(a) is the stress-time curves of the maximum stress point of the two stents during the whole shape memory process. The curve trends of the two stents were similar. In the programming stage, the stress increased with time. During the cooling stage, the stress increased rapidly with temperature, and the stress dropped sharply after removing the load. When reheated, the stent returned from temporary shape to the original shape (permanent shape) due to the release of storage strain. Therefore, the stress and strain in the recovery stage decrease gradually with time. The maximum stresses of the two stents were 28.37 and 35.27 MPa, respectively, which were less than the strength of the shape memory PLA material (Figure 3(a), 61.5 MPa), so the safety of the stents was verified. Figure 7(b) is the strain-time curves of the maximum stress point in the stents. During the programming process, the strain of the two stents increased dramatically. After removing the external loads, the stents produced a certain elastic recovery and the strain decreased slightly. Compared with the Type 1 stent, the Type 2 stent had a larger maximum strain and a slower recovery process due to more constituent units (Figure 4).

2.4 Deployment simulation of stents within blood vessel

To examine whether the vascular stent can expand the blocked blood vessel in the physical microenvironment, the deployment process of the stent in the blood vessel was simulated by ABAQUS. The blood vessels were calculated using shell cells, and the interaction between the blood vessels and the stents was set as hard contact. The results showed that both vascular stents were able to expand the narrow vessels (Figure 8). The maximum stresses of the two stents were 3.94 and 3.15 MPa, respectively. Comparing the two vascular stents, the Type 2 vascular stent can expand the blood vessels more uniformly and the blood vessel wall was smoother than that of the Type 1 stent (Figure 8(e) and (f)), which was because of the different topologies.

3 Experimental

3.1 Details of stents fabrication

Shape memory PLA particles (M_w=100000) were extruded through a twin-screw extruder (CTE20 PLUS, Coperion Nanjing Machinery Co., Ltd) to fabricate printing filaments

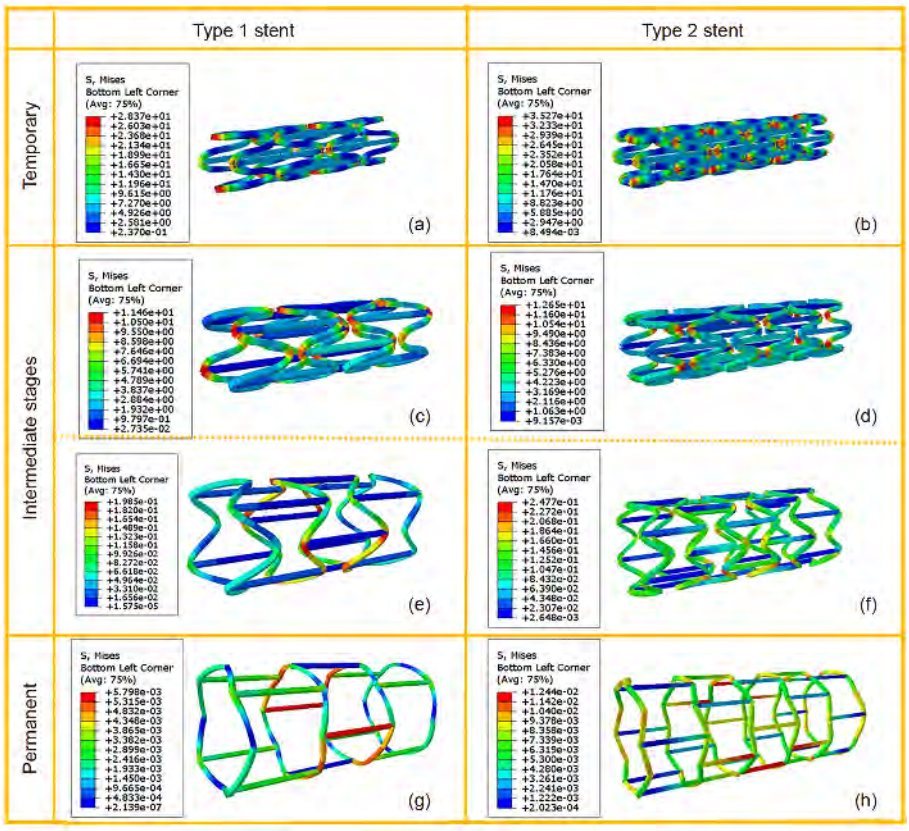

Figure 6 (Color online) Shape memory recovery process: temporary shape of Type 1 (a) and Type 2 (b) stents; (c)–(f) intermediate stages of recovery process; permanent shape of Type 1 (g) and Type 2 (h) stents.

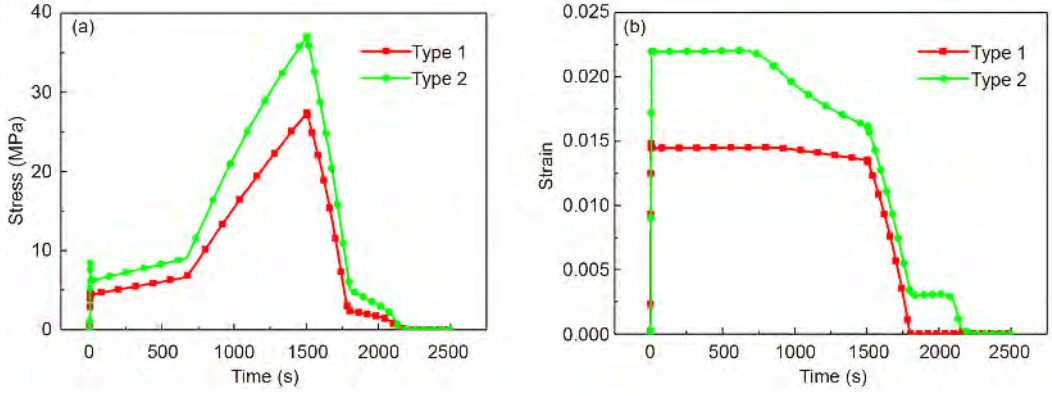

Figure 7 (Color online) (a) Stress-time curves and (b) strain-time curves during the shape memory simulation process.

at 200°C. The screw diameter and screw speed were 1.75 mm and 200 r/min, respectively. Taking the accuracy of the printer into account, the enlarged models of the stents were constructed on SolidWorks software. To ensure consistency of size of the two stents as much as possible, the Type 1 stent was enlarged eight times, and the Type 2 was enlarged seven times. The modeling process of the two types of stents was as follows: first, planar geometries with different NPR structures were constructed, as shown in Figure 4 (a) and (d). The planar geometries were then bent into three-dimensional tubular stents (Figure 4(b) and (e)). After construction, the models were exported as printable STL files and were printed through a 3D printer (Anycubic i3 Mega, Zhejiang, China) with a nozzle diameter of 0.4 mm, a temperature of 190°C and a printing speed 5 mm/min by fused deposition modeling (FDM). Figure 4(e) and (f) depicts the printed stents with different numbers of NPR structural units. The diameters of Type 1 stent and Type 2 stent were 12.79 and 13.99 mm, while the lengths were 40.80 and 44.11 mm, respectively.

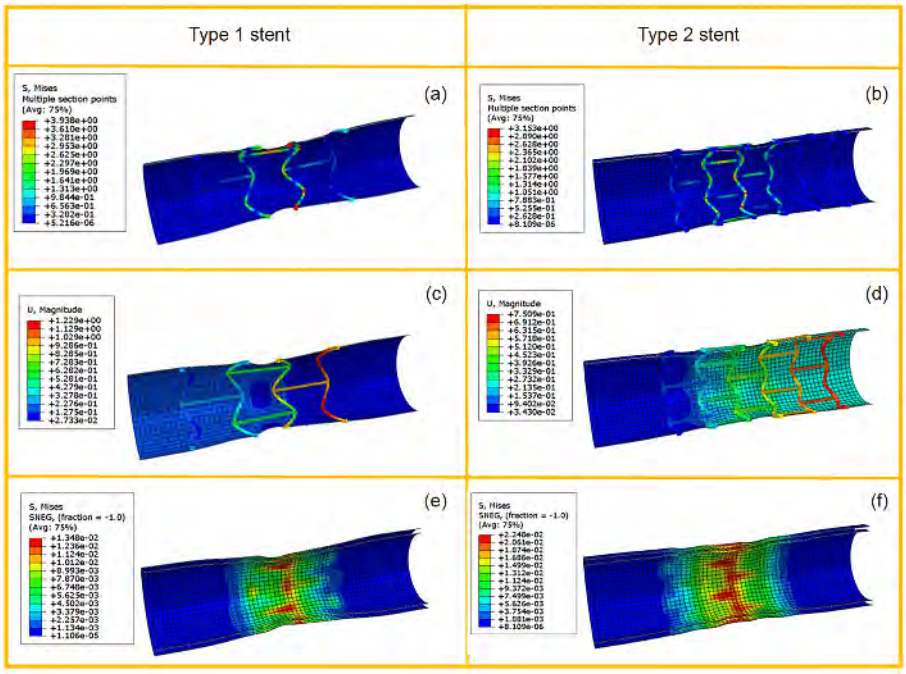

Figure 8 (Color online) Deployment simulation of stents within blood vessels. (a), (b) Stress distribution of vessels and stents; (c), (d) displacement distribution of vessels and stents; (e), (f) stress distribution of vessels.

3.2 Mechanical performances

Dumbbell-shaped samples for uniaxial tensile tests were printed according to ASTM D638 with dimensions of 115 mm×6 mm×2 mm [45]. Axial and radial compression (ASTM D2412 standard) tests for stents were performed on a tensile tester equipped with 200 N load cell and the loading rate was 1 mm/min [46]. Three-point bending tests for stents were performed with a constant span length of 25 mm until failure. All mechanical tests were performed using a Zwick/Roell Z010 at room temperature. In each case, a preload of 0.5 N was applied and three samples were tested to obtain an average value. The fracture surface morphologies of the samples were studied by VEGA3 TESCAN scanning electron microscope (SEM) with an accelerating voltage of 20.0 kV.

3.3 Shape memory properties

For experiments, the stent was placed in hot water (70°C) and compressed to a small volume. Then the compressed stent was placed in the hot water again to examine the shape memory property, and the shape recovery process was recorded.

3.4 *In vitro* feasibility study

The experimental deployment process was performed in the phosphate-buffered saline (PBS) buffer solution. The deployment was carried out at 70°C, taking the effect of temperature on the pH into account, the pH of PBS buffer was adjusted to between 7.35 and 7.40 (within the blood pH range). This process was as follows: first, the stent was compressed, then the compressed stent was implanted into the stenotic simulated blood vessel; finally, the stent loaded into simulated blood vessel was placed in the PBS buffer to simulate the deployment process *in vivo*.

4 Results and discussion

4.1 Mechanical properties

To ensure the stents can provide sufficient support for vascular stenosis, axial tensile load, compressive load and radial load were applied to examine their mechanical performances. Figure 9(a) shows the axial compression tests of the stents. The maximum load of the Type 1 stent was about 57 N, and the Type 2 stent was about 53 N; the maximum displacements were 2.4 and 2.8 mm, respectively. Both maximum load and maximum displacement of the Type 1 stent were higher than that of the Type 2 stent due to different topology structure. The Type 1 stent had a "large but sparse" structure, meaning that the structural unit size was large, but the overall number of units was small. As displayed in Figure 4(a), the case of the Type 2 stent was the opposite, it had a "small but dense" structure (Figure 4(b)). Therefore, the larger structural unit with NPR structure in the Type 1 stent can sustain a larger displacement, and the thickness of the

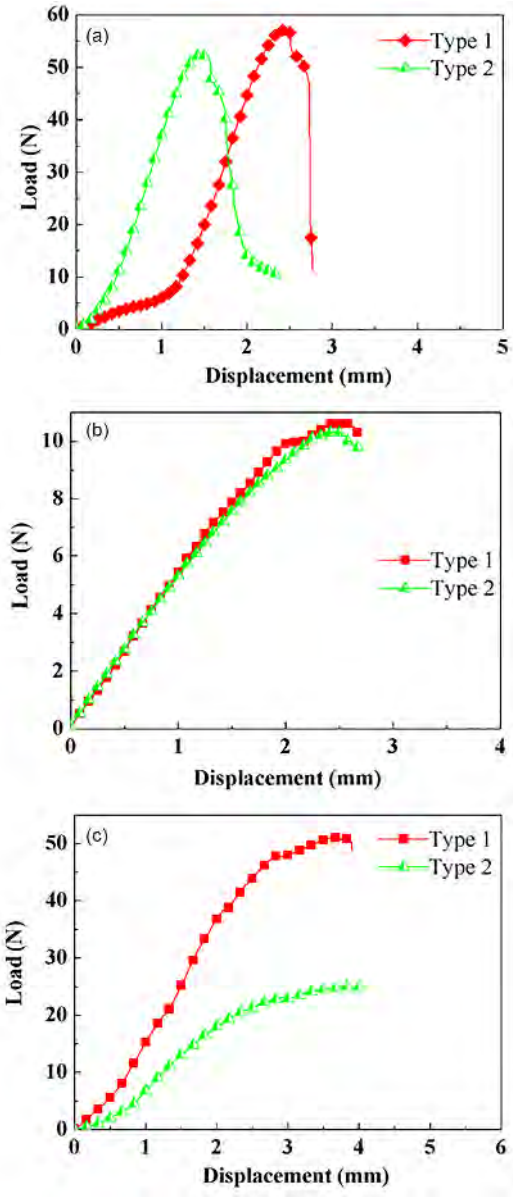

Figure 9 (Color online) Mechanical behaviors of shape memory stents. (a) Axial compression tests; (b) radial compression tests; (c) three-point bending tests.

unit was responsible for the maximum load. Similarly, in radial compression tests (Figure 9(b)), the maximum load of the Type 1 stent was also higher than that of Type 2 stent, but the gap between the two increased. The maximum load of the Type 1 stent was 50 N, which was twice that of the Type 2 stent. The maximum loads of the two stents were higher than the value in ref. [47]. In clinical applications, flexibility is also needed for stents. And three-point bending test is a measurement of flexibility. As demonstrated in Figure 9(c), the three-point bending curves of the two types of stents were almost the same, which indicated that they had similar flexibility. In addition, the maximum load and displacement of the two stents were also higher than the values in the literature [48]. It was worth to note that the surface coverages of the two stents were only about 21%, therefore, their mechanical properties were quite outstanding. Figure 10(a)–(c) displays the fracture surface morphologies of the samples. The failures of the stents occurred primarily at three locations, including the separation between longitudinal printed layers (Figure 10(a)), lateral fractures (Figure 10(b)), and fractures at lateral and longitudinal contacts (Figure 10(c)).

4.2 Shape memory properties

The shape recovery properties of stents were evaluated by diameter recovery ratio (R_{rD}) and length recovery ratio (R_{rL}), which are defined as follows:

$$R_{rD} = \left(1 - \frac{D_0 - D}{D_0}\right) \times 100\%, \tag{10}$$

$$R_{rL} = \left(1 - \frac{L_0 - L}{L_0}\right) \times 100\%, \tag{11}$$

where D_0 is the initial diameter, D is the diameter after recovery. L_0 is the initial length, L is the length after recovery.

According to the finite element analysis and experiments, the shape recovery ratios of the diameter and length are shown in Figure 11(a), and the recovery ratio of both stents exceeded 94%, which indicated excellent shape memory performances. Figure 11(b) shows the shape recovery ratios versus time curves of the two stents based on experiments. The glass transition temperature (T_g) of the shape memory PLA was around 66°C according to the differential scanning calorimeter (DSC) diagram (Figure S5), and the recovery temperature was 70°C. Large volume changing rate, high recovery ratio (both are above 98%) and high recovery speed can be observed (Supporting Information Videos S1 and S2). The Type 1 stent can return from the temporary shape to the original shape within 3 s. The Type 2 stent completed the recovery within 5 s. It is worth noting that Tamai et al. [49] applied biodegradable polymer stents to human coronary artery for the first time in 2000. The stent was expanded by balloon dilatation at 80°C. And the patients were followed up for 6 months. This study confirmed the feasibility and safety of the stent and the method. Therefore,a slightly higher temperature of SMPs stents for only a few seconds will not cause blood vessel injury seriously. In addition, the recovery speed of the Type 1 stent was faster than that of the Type 2 stent due to fewer constituent units, which was consistent with the simulation results (Figure 7(b)).

4.3 *In vitro* feasibility study

The vascular wall and the intestinal wall have similar components, such as muscle fibers and connective tissue, therefore, the sheep intestine was selected as a simulated blood vessel for the *in vitro* feasibility test. To simulate the de-

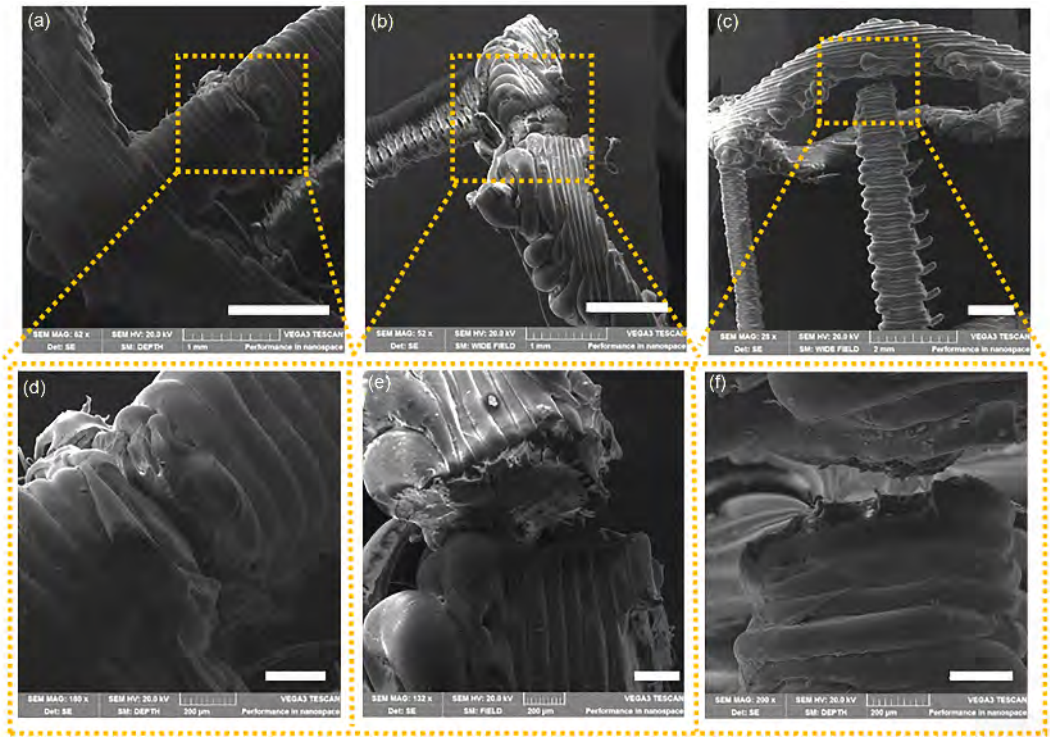

Figure 10 (Color online) (a)–(c) SEM fracture morphologies of stents at different locations; (d)–(f) their partially enlarged SEM images. The scale bar is 1 mm in (a)–(c), and the scale bar is 200 μm in (d)–(f).

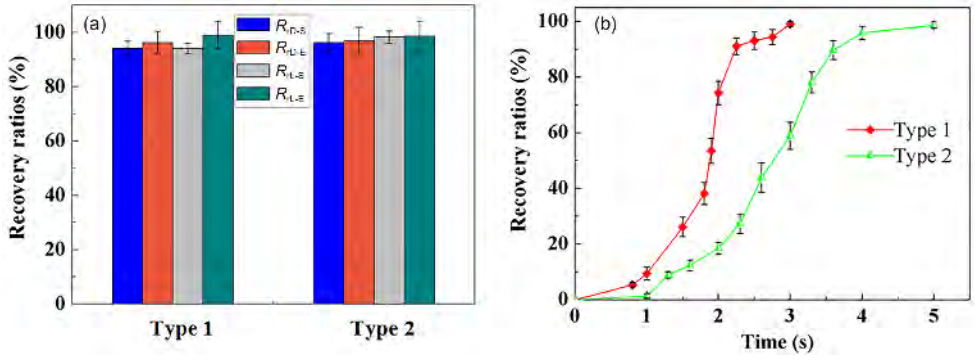

Figure 11 (Color online) (a) Diameter and length recovery ratio of the two stents: $R_{rD\text{-}S}$ represents the diameter recovery ratio based on simulations; $R_{rD\text{-}E}$ represents the diameter recovery ratio based on experiments; $R_{rL\text{-}S}$ represents the length recovery ratio based on simulations; $R_{rL\text{-}E}$ represents the length recovery ratio based on experiments; (b) recovery ratio versus time curves.

ployment process of the stent in the physical microenvironment more realistically, PBS solution was selected as the feasibility test medium. The osmotic pressure and the ion concentration of PBS solution are similar to those of the human body, and the pH value can be maintained close to that of human body. The deployment processes are shown in Supporting Information Videos S3 and S4. As demonstrated in Figure 12, the vascular stents can overcome the resistance of the vascular wall to expand it. The recovery ratio of the Type 2 stent (around 95%) was higher than that of the Type 1 stent (around 91%). And it took only 4 s for the Type 1 stent to expand the simulated blood vessel and 5 s for the Type 2 stent. Such rapid recovery processes can make the implantation process more effective.

5 Conclusions

In conclusion, two types of 4D printed personalized shape memory stents with negative Poisson's ratio structure were designed and optimized. Mechanical tests, shape memory performance tests and feasibility tests *in vitro* were conducted. Shape recovery experimental tests showed that the recovery ratios of the two types of stents were as high as 98%. With only 21% surface coverage, the *in vitro* feasibility study in the simulated body fluid indicated that both stents

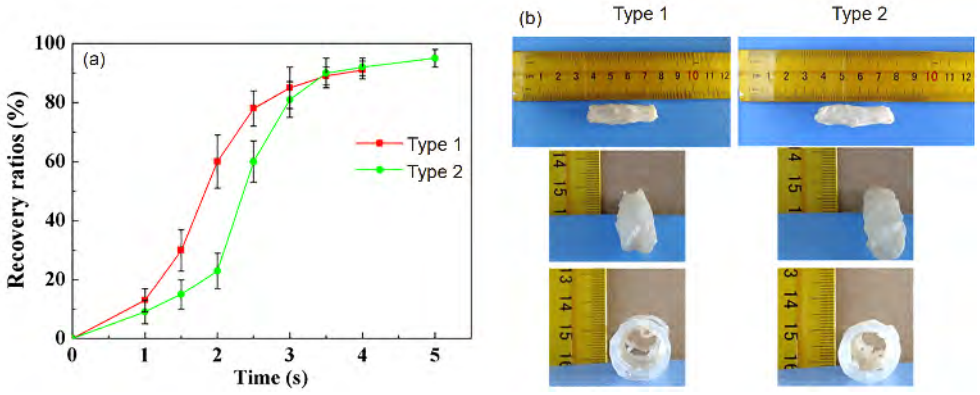

Figure 12 (Color online) (a) Stents recovery ratios versus time curves in the simulated blocked vessels; (b) feasibility *in vitro*: the two types of stents before and after expanding the narrow simulated blood vessels.

were able to expand the narrow blood vessel within 5 s. However, the shape memory stents also have some limitations. The T_g of the shape memory PLA is a little high although it would not cause vessel injury seriously according to Tamai's pioneer work. Some studies are also needed to reduce the T_g of shape memory PLA, such as modifying with low molecular modifiers [14], or preparing copolymers [50]. Therefore, 4D printed shape memory stents with negative Poisson's ratio structure have great prospects for the treatment of vascular stenosis and some work still needs to be done in the future.

This work was supported by the National Natural Science Foundation of China (Grant Nos. 11632005 and 11672086). The authors thank Dr. Fenghua Zhang for her valuable advice and Xiaozhou Xin for his kind help.

Supporting Information

The supporting information is available online at tech.scichina.com and link.springer.com. The supporting materials are published as submitted, without typesetting or editing. The responsibility for scientific accuracy and content remains entirely with the authors.

1 Leng J, Lan X, Liu Y, et al. Shape-memory polymers and their composites: Stimulus methods and applications. Prog Mater Sci, 2011, 56: 1077–1135
2 Mu T, Liu L, Lan X, et al. Shape memory polymers for composites. Compos Sci Tech, 2018, 160: 169–198
3 Wang J, Zhao Q, Cui H, et al. Tunable shape memory polymer mold for multiple microarray replications. J Mater Chem A, 2018, 6: 24748–24755
4 Zhao Q, Wang Y, Cui H, et al. Bio-inspired sensing and actuating materials. J Mater Chem C, 2019, 7: 6493–6511
5 Yakacki C M, Shandas R, Safranski D, et al. Strong, tailored, biocompatible shape-memory polymer networks. Adv Funct Mater, 2008, 18: 2428–2435
6 Yakacki C M, Shandas R, Lanning C, et al. Unconstrained recovery characterization of shape-memory polymer networks for cardiovascular applications. Biomaterials, 2007, 28: 2255–2263
7 Yakacki C M, Gall K. Shape-memory polymers for biomedical applications. In: Shape-Memory Polymers. Lendlein A, ed. Berlin-Heidelberg: Springer, 2010. 147–175
8 Wischke C, Neffe A T, Steuer S, et al. Evaluation of a degradable shape-memory polymer network as matrix for controlled drug release. J Control Release, 2009, 138: 243–250
9 Lendlein A, Langer R. Biodegradable, elastic shape-memory polymers for potential biomedical applications. Science, 2002, 296: 1673–1676
10 Balk M, Behl M, Wischke C, et al. Recent advances in degradable lactide-based shape-memory polymers. Adv Drug Deliver Rev, 2016, 107: 136–152
11 Chen J, Hu J, Leung A K L, et al. Shape memory ankle-foot orthoses. ACS Appl Mater Interfaces, 2018, 10: 32935–32941
12 Baker R M, Tseng L F, Iannolo M T, et al. Self-deploying shape memory polymer scaffolds for grafting and stabilizing complex bone defects: A mouse femoral segmental defect study. Biomaterials, 2016, 76: 388–398
13 Zhang D, George O J, Petersen K M, et al. A bioactive "self-fitting" shape memory polymer scaffold with potential to treat cranio-maxillo facial bone defects. Acta Biomater, 2014, 10: 4597–4605
14 Zhao Q, Wang J, Cui H, et al. Programmed shape-morphing scaffolds enabling facile 3D endothelialization. Adv Funct Mater, 2018, 28: 1801027
15 Bose S, Vahabzadeh S, Bandyopadhyay A. Bone tissue engineering using 3D printing. Mater Today, 2013, 16: 496–504
16 Wang M O, Vorwald C E, Dreher M L, et al. Evaluating 3D-printed biomaterials as scaffolds for vascularized bone tissue engineering. Adv Mater, 2015, 27: 138–144
17 Yang B, Yin J, Chen Y, et al. 2D-black-phosphorus-reinforced 3D-printed scaffolds: A stepwise countermeasure for osteosarcoma. Adv Mater, 2018, 30: 1705611
18 Deng C, Yao Q, Feng C, et al. 3D printing of bilineage constructive biomaterials for bone and cartilage regeneration. Adv Funct Mater, 2017, 27: 1703117
19 Zhuang P, Sun A X, An J, et al. 3D neural tissue models: From spheroids to bioprinting. Biomaterials, 2018, 154: 113–133
20 Norman J, Madurawe R D, Moore C M V, et al. A new chapter in pharmaceutical manufacturing: 3D-printed drug products. Adv Drug Deliver Rev, 2017, 108: 39–50
21 Sadia M, Arafat B, Ahmed W, et al. Channelled tablets: An innovative approach to accelerating drug release from 3D printed tablets. J Control Release, 2018, 269: 355–363
22 Lin M, Firoozi N, Tsai C T, et al. 3D-printed flexible polymer stents for potential applications in inoperable esophageal malignancies. Acta Biomater, 2019, 83: 119–129
23 Wei H, Zhang Q, Yao Y, et al. Direct-write fabrication of 4D active shape-changing structures based on a shape memory polymer and its nanocomposite. ACS Appl Mater Interfaces, 2017, 9: 876–883
24 Truby R L, Wehner M, Grosskopf A K, et al. Soft somatosensitive actuators via embedded 3D printing. Adv Mater, 2018, 30: 1706383
25 Lei D, Yang Y, Liu Z, et al. A general strategy of 3D printing thermosets for diverse applications. Mater Horiz, 2019, 6: 394–404
26 Miao S, Castro N, Nowicki M, et al. 4D printing of polymeric ma-

terials for tissue and organ regeneration. Mater Today, 2017, 20: 577–591
27 Momeni F, M.Mehdi Hassani.N S, Liu X, et al. A review of 4D printing. Mater Des, 2017, 122: 42–79
28 Zarek M, Mansour N, Shapira S, et al. 4D printing of shape memory-based personalized endoluminal medical devices. Macromol Rapid Commun, 2017, 38: 1600628
29 Im S H, Jung Y, Kim S H. Current status and future direction of biodegradable metallic and polymeric vascular scaffolds for next-generation stents. Acta Biomater, 2017, 60: 3–22
30 Sigwart U, Puel J, Mirkovitch V, et al. Intravascular stents to prevent occlusion and re-stenosis after transluminal angioplasty. N Engl J Med, 1987, 316: 701–706
31 Wiebe J, Nef H M, Hamm C W. Current status of bioresorbable scaffolds in the treatment of coronary artery disease. J Am College Cardiology, 2014, 64: 2541–2551
32 Zhao Q, Cui H, Wang J, et al. Regulation effects of biomimetic hybrid scaffolds on vascular endothelium remodeling. ACS Appl Mater Interfaces, 2018, 10: 23583–23594
33 Kulkarni R P, Bellamy E A. A new thermo-expandable shape-memory nickel-titanium alloy stent for the management of ureteric strictures. BJU Int, 2001, 83: 755–759
34 Fu M, Liu F, Hu L. A novel category of 3D chiral material with negative Poisson's ratio. Compos Sci Tech, 2018, 160: 111–118
35 Huang J, Zhang Q, Scarpa F, et al. Multi-stiffness topology optimization of zero Poisson's ratio cellular structures. Compos Part B-Eng, 2018, 140: 35–43
36 Park S A, Lee S J, Lim K S, et al. *In vivo* evaluation and characterization of a bio-absorbable drug-coated stent fabricated using a 3D-printing system. Mater Lett, 2015, 141: 355–358
37 Pacharra S, Ortiz R, McMahon S, et al. Surface patterning of a novel PEG-functionalized poly-l-lactide polymer to improve its biocompatibility: Applications to bioresorbable vascular stents. J Biomed Mater Res, 2019, 107: 624–634
38 Adeli H, Cheng N. Integrated genetic algorithm for optimization of space structures. J Aerospace Eng, 1993, 6: 315–328
39 Kociecki M, Adeli H. Two-phase genetic algorithm for topology optimization of free-form steel space-frame roof structures with complex curvatures. Eng Appl Artificial Intelligence, 2014, 32: 218–227
40 Gibson L J, Ashby M F, Schajer G S, et al. The mechanics of two-dimensional cellular materials. Proc R Soc A-Math Phys Eng Sci, 1982, 382: 25–42
41 Abouhamze M, Shakeri M. Multi-objective stacking sequence optimization of laminated cylindrical panels using a genetic algorithm and neural networks. Composite Struct, 2007, 81: 253–263
42 He Y, Guo S, Liu Z, et al. Pattern transformation of thermo-responsive shape memory polymer periodic cellular structures. Int J Solids Struct, 2015, 71: 194–205
43 Yu K, Li H, McClung A J W, et al. Cyclic behaviors of amorphous shape memory polymers. Soft Matter, 2016, 12: 3234–3245
44 Hager M D, Bode S, Weber C, et al. Shape memory polymers: Past, present and future developments. Prog Polym Sci, 2015, 49-50: 3–33
45 ASTM Standard. D638-97. Standard Test Method for Tensile Properties of Plastics. American Society for Testing and Materials, New York, 1997
46 ASTM Standard. D2412-02. Standard Test Method for Determination of External Loading Characteristics of Plastic Pipe by Parallel-Plate Loading. ASTM International, West Conshohocken, 2002
47 Chen M C, Liu C T, Tsai H W, et al. Mechanical properties, drug eluting characteristics and *in vivo* performance of a genipin-cross-linked chitosan polymeric stent. Biomaterials, 2009, 30: 5560–5571
48 Wang Q, Fang G, Zhao Y, et al. Computational and experimental investigation into mechanical performances of poly-l-lactide acid (Plla) coronary stents. J Mech Behav BioMed Mater, 2017, 65: 415–427
49 Tamai H, Igaki K, Kyo E, et al. Initial and 6-month results of biodegradable poly-*l*-lactic acid coronary stents in humans. Circulation, 2000, 102: 399–404
50 Wong Y S, Salvekar A V, Zhuang K D, et al. Bioabsorbable radiopaque water-responsive shape memory embolization plug for temporary vascular occlusion. Biomaterials, 2016, 102: 98–106